

Predictability crisis in inflationary cosmology and its resolution

Vitaly Vanchurin, Alexander Vilenkin

Institute of Cosmology, Department of Physics, Tufts University, Medford MA 02155, USA

and

Serge Winitzki

DAMTP, University of Cambridge, Cambridge CB3 9EW, UK

In memory of Chandra Pathinayake

Abstract

Models of inflationary cosmology can lead to variation of observable parameters (“constants of Nature”) on extremely large scales. The question of making probabilistic predictions for today’s observables in such models has been investigated in the literature. Because of the infinite thermalized volume resulting from eternal inflation, it has proven difficult to obtain a meaningful and unambiguous probability distribution for observables, in particular due to the gauge dependence. In the present paper, we further develop the gauge-invariant procedure proposed in a previous work for models with a continuous variation of “constants”. The recipe uses an unbiased selection of a connected piece of the thermalized volume as sample for the probability distribution. To implement the procedure numerically, we develop two methods applicable to a reasonably wide class of models: one based on the Fokker-Planck equation of stochastic inflation, and the other based on direct simulation of inflationary spacetime. We present and compare results obtained using these methods.

I. INTRODUCTION

The parameters we call “constants of Nature” may in fact be variables related to some slowly varying fields. For example, what we perceive as a cosmological constant could be a potential $U(\chi)$ of some field $\chi(x)$. If this potential is very flat, so that the evolution of χ is much slower than the Hubble expansion, then observations will not distinguish between $U(\chi)$ and a true cosmological constant. Observers in different parts of the universe could then measure different values of $U(\chi)$.

Spatial variation of the fields χ_a associated with the “constants” can naturally arise in the framework of inflationary cosmology [1]. The dynamics of light scalar fields during inflation are strongly influenced by quantum fluctuations, so different regions of the universe

thermalize with different values of χ_a . An intriguing question is whether or not we can predict the values of the “constants” we are most likely to observe.

It is important to realize that this question arises not only in some exotic models especially designed to have variable constants. On the contrary, we have to face it in *all* inflationary models attempting to predict the spectrum of cosmological density fluctuations. The density fluctuation $\delta\rho/\rho(l)$ is determined by the quantum fluctuation $\delta\phi(l)$ of the inflaton field ϕ at the time when the corresponding length scale l crossed the horizon. Different realizations of random fluctuations $\delta\phi(l)$ result in different density fluctuation spectra in widely separated parts of the universe. [In this case, the fluctuations $\delta\phi(l)$ on different scales play the role of the fields χ_a .] The question is then what spectrum $\delta\rho/\rho(l)$ we are most likely to observe in our neighborhood? In more general terms, we would like to determine the probability distribution $\mathcal{P}(\chi)$ for the fields χ_a associated with variable constants.

The inflationary scenario implies a very large universe inhabited by numerous civilizations that will measure different values of χ_a . We can define the probability $\mathcal{P}(\chi)d\chi_1\dots d\chi_n$ for χ_a to be in the intervals $d\chi_a$ as being proportional to the number of civilizations which will measure χ_a in that interval [2]. This includes all present, past and future civilizations; in other words, it is the number of civilizations throughout the entire spacetime, rather than at a particular moment of time. Assuming that we are a typical civilization, we can expect to observe χ_a near the maximum of $\mathcal{P}(\chi)$ [3]. The assumption of being typical has been called the “principle of mediocrity” in Ref. [2].

An immediate objection to this approach is that we are ignorant about the origin of life, let alone intelligence, and therefore the number of civilizations cannot be calculated. However, the approach can still be used to find the probability distribution for parameters which do not affect the physical processes involved in the evolution of life. The cosmological constant Λ , the density parameter Ω and the amplitude of density fluctuations Q are examples of such parameters. We shall assume that our fields χ_a belong to this category. The probability for a civilization to evolve on a suitable planet is then independent of χ_a , and instead of the number of civilizations we can use the number of habitable planets or, as a rough approximation, the number of galaxies. [We are assuming that civilizations can exist only for a finite period of time after inflation, either because the stars run out of nuclear fuel and die, or because protons eventually decay. A galaxy then gives rise to a finite average number of civilizations.] Thus, we can write

$$\mathcal{P}(\chi)d^n\chi \propto d\mathcal{N}, \tag{1}$$

where $d\mathcal{N}$ is the number of galaxies that are going to be formed in regions where χ_a take values in the intervals $d\chi_a$.

The meaning of Eq. (1) is unambiguous in models where the total number of galaxies in the universe is finite. Otherwise, one has to introduce some cutoff and define the ratio of probabilities for the intervals $d^n\chi^{(1)}$ and $d^n\chi^{(2)}$ as the ratio of the galaxy numbers $d\mathcal{N}^{(1)}/d\mathcal{N}^{(2)}$ in the limit when the cutoff is removed. The situation is relatively straightforward in the case of an infinite universe which is more or less homogeneous on very large scales. One can then evaluate the ratio $d\mathcal{N}^{(1)}/d\mathcal{N}^{(2)}$ in a large comoving volume \mathcal{V} and then take the limit as $\mathcal{V} \rightarrow \infty$. The result is expected to be independent of the limiting procedure; for example, it should not depend on the shape of the volume \mathcal{V} . (It is assumed, however, that the volume selection is unbiased, that is, that the volume \mathcal{V} is not carved to

favor some values of χ_a at the expense of other values.)

The problem is much more serious in models of eternal inflation where the universe is never completely thermalized [6,7]. In such models, the volumes of both inflating and thermalized regions grow exponentially with time and the number of galaxies grows without bound, even in a region of a finite comoving size. One can deal with this problem by introducing a time cutoff and including only regions that thermalized prior to some moment of time t_c , with the limit $t_c \rightarrow \infty$ at the end. One finds, however, that the resulting probability distributions are extremely sensitive to the choice of the time coordinate t [4]. This applies in particular to the calculations of the density fluctuation spectra. Having chosen t to be the proper time along the world lines of comoving observers, Linde, Linde and Mezhlumian [8] found that a typical observer could find herself near the center of a very deep minimum of the density field. On the other hand, if one uses the expansion factor along the trajectories as the time coordinate, one recovers the standard results [9]. Coordinates in General Relativity are arbitrary labels, and such gauge dependence of the results casts doubt on any conclusion reached using this approach.

An alternative procedure, suggested in [10], is to introduce a χ -dependent cutoff at the time $t_c(\chi)$, when all but a small fraction ϵ of the comoving volume destined to thermalize with χ_a in the intervals $d\chi_a$ has thermalized. The limit $\epsilon \rightarrow 0$ is taken after calculating the probabilities. It was shown in [10,11] that the resulting probability distribution is essentially insensitive to the choice of time parametrization. However, the same problem appears in a different guise. Linde and Mezhlumian [12] have found a family of gauge-invariant cutoff procedures which includes the ϵ -procedure described above. All these procedures give vastly different results for the probability distributions.

In the face of these difficulties, serious doubts have been expressed that a meaningful definition of probabilities in an eternally inflating universe is even in principle possible [4,5,12]. Once again, this problem cannot be brushed aside as “exotica” because inflation is eternal in practically all models suggested so far. Eternal inflation is generic; it is finite inflation that is exotic. We believe, therefore, that the situation deserves to be called the “predictability crisis in inflationary cosmology”.

In this paper we are going to analyze the resolution of the crisis suggested by one of us in Ref. [13]. We begin, in Section II, by discussing the spacetime structure of an eternally inflating universe. This will help us clarify the origin of the problem and will motivate its resolution proposed in Section III. In the following Sections IV – V we develop methods for calculating probabilities based on the prescription introduced in Section III. The first method uses the Fokker-Planck equation of stochastic inflation. In Section IV we derive the appropriate form of the equation, discuss the initial conditions, and work out some examples. The second method uses numerical simulations of eternal inflation. In Section V we describe our simulations and compare them to previous work. We also compare the results obtained from the simulations with those obtained using the Fokker-Planck equation. Our conclusions are summarized in Section VI.

II. SPACETIME STRUCTURE AND GAUGE DEPENDENCE OF PROBABILITIES

An inflating Universe can be locally described using the synchronous coordinates,

$$ds^2 = d\tau^2 - a^2(\mathbf{x}, \tau)d\mathbf{x}^2. \quad (2)$$

The lines of $\mathbf{x} = \text{const}$ in this metric are timelike geodesics corresponding to the worldlines of co-moving observers, and the coordinate system is well defined as long as the geodesics do not cross. This will start happening only after thermalization, when matter in some regions will start collapsing as a result of gravitational instability. Hence, the synchronous coordinates (2) can be extended to the future well into the thermalized region.

A. Double-well model

We shall first consider the simplest situation when there is a single inflaton field ϕ with a double-well potential, as in Fig. 1, and no other fields χ_a . The potential in the figure is symmetric with respect to $\phi \rightarrow -\phi$, although this is not essential. Depending on quantum fluctuations, an inflating region with $\phi \approx 0$ near the maximum of the potential can thermalize in either of the two minima at $\phi = \pm\eta$. The two minima may correspond to different physics, in which case this is an example of a model where the constants of Nature can take a discrete set of values.

In the slow-roll regime of inflation, the field ϕ is a slowly-varying function of the coordinates, so that spatial gradients of ϕ can be neglected and

$$\dot{\phi}^2 \ll 2V(\phi). \quad (3)$$

The classical evolution of the scale factor $a(\mathbf{x}, \tau)$ and of the inflaton $\phi(\mathbf{x}, \tau)$ is then described by the equations

$$(\dot{a}/a)^2 \equiv H^2 \approx 8\pi V(\phi)/3, \quad (4)$$

$$\dot{\phi} \approx -V'(\phi)/3H = -H'(\phi)/4\pi, \quad (5)$$

where dots represent derivatives with respect to τ and we use the Planck units, $\hbar = c = G = 1$. With the aid of Eqs. (4),(5), the slow-roll condition (3) can be expressed as

$$H' \ll 6H. \quad (6)$$

This condition is violated near the points $\phi = \phi_*^{(j)}$, signalling the end of inflation. The slow variation of ϕ implies that H is also a slowly-varying function of \mathbf{x} and τ , and thus the spacetime is locally close to de Sitter, with a horizon length H^{-1} .

Quantum fluctuations of the field ϕ can be pictured as a ‘random walk’ [superimposed on the classical motion (5)] in which ϕ undergoes random steps of *rms* magnitude $(\delta\phi)_{\text{rms}} = H/2\pi$ per Hubble time, $\delta\tau = H^{-1}$. The fluctuations $\delta\phi$ are correlated on the scale of the horizon ($l \sim H^{-1}$), but correlations rapidly decay with distance and become totally negligible on the scale of a few horizons. The fluctuations are dynamically unimportant if the classical ‘velocity’ $|\dot{\phi}|$ is much greater than the characteristic speed of the random walk, $(\delta\phi)_{\text{rms}}/\delta\tau = H^2/2\pi$, which gives

$$H' \gg H^2. \quad (7)$$

This condition is violated in the region $\varphi_q^{(1)} < \varphi < \varphi_q^{(2)}$ near the top of the potential (see Fig. 1). The dynamics of φ in this region is dominated by quantum fluctuations. The deterministic slow-roll regions are bounded by the values $\varphi_q^{(j)}$ and $\varphi_*^{(j)}$, $j = 1, 2$.

The random-walk picture of quantum fluctuations can be used in numerical simulations of eternal inflation [14,4]. To illustrate the spacetime structure of an eternally inflating universe, we have performed simulations for several models in one and two spatial dimensions, with and without the additional fields χ_a . The details of the simulations are given in Section V. Fig. 2 shows the distribution of inflating and thermalized regions in two dimensions at four consecutive moments of time for the single-inflaton model with a double-well potential. The form of the potential is taken to be

$$V(\varphi) = V_0 \cos^2(\alpha\varphi), \quad (8)$$

where $\alpha = \pi/2\eta$; we only consider the range $-\eta < \varphi < \eta$. With $\alpha \lesssim 1$ and $H_0/\alpha \lesssim 1$, we have

$$\varphi_q^{(1,2)} \sim \pm H_0/\alpha^2, \quad (9)$$

where $H_0 = H(\varphi = 0) = (8\pi V_0/3)^{1/2}$, and

$$\varphi_*^{(1,2)} \approx \pm(\eta - 1/6). \quad (10)$$

In the simulations we used $V_0 = 0.05$ and $\alpha = 1$. Our choice of parameters in most of the simulations was dictated by the computational constraints (see Sec. V), so we made no attempt to make this choice realistic.

There are two types of thermalized regions in the model (8) (corresponding to the two minima of the potential at $\varphi = \pm\eta$) which are shown with different shades of grey. Thermalized regions of different type can never merge; they are always separated by inflating regions (shown in white) which can be thought of as inflating domain walls [15]. This is an example of topological inflation. Thermalized regions of the same type can also be separated by inflating regions, but there is nothing to prevent these regions from merging, and we can see from the sequence in Fig. 2 that neighboring regions of the same type do tend to merge.

As time goes on, more and more comoving volume gets thermalized, and at $\tau \rightarrow \infty$ only a vanishing fraction of the initial volume is still inflating. However, the physical volume of the inflating regions grows exponentially with time. Geometrically, these regions form a fractal of dimension $d < 3$ [14].

A spacetime slice through the universe (in the $x - \tau$ “plane”) is shown in Fig. 3. The simulation starts with a horizon-size region and a homogeneous field $\varphi = 0$ at $\tau = 0$ (bottom of the figure). We shall be particularly interested in the thermalization hypersurfaces $\Sigma_*^{(j)} : \varphi = \varphi_*^{(j)}$ which separate inflating and thermalized spacetime regions. We see from the figure that these surfaces tend to become asymptotically static in the comoving coordinates as $\tau \rightarrow \infty$. This does not mean, however, that the surfaces become timelike at large τ . To picture the geometry of these surfaces, one has to keep in mind that physical lengths in an inflating universe are related to coordinate differences by an exponentially growing scale factor. As a result, the boundaries of thermalized regions (as well as all surfaces of constant φ in the slow-roll regime) are spacelike, and are in fact very flat.

The spacelike character of the constant- φ surfaces can be understood as follows [10]. Consider the normal vector to the surfaces, $\partial_\mu\varphi$. We have

$$\partial_\mu\varphi\partial^\mu\varphi = \dot{\varphi}^2 - a^{-2}(\nabla\varphi)^2. \quad (11)$$

The spatial gradients of φ are caused by quantum fluctuations. On the scale of the horizon, the gradient is of the order $a^{-1}|\nabla\varphi| \sim (\delta\varphi)_{\text{rms}}/H^{-1} \sim H^2/2\pi$, and is even smaller on larger scales. On the other hand, from Eqs. (5),(7), $|\dot{\varphi}| \gg H^2/2\pi$. Hence, $\partial_\mu\varphi\partial^\mu\varphi > 0$, and the surfaces $\varphi = \text{const}$ are spacelike.

In general, thermalization hypersurfaces $\Sigma_*^{(j)}$ cannot terminate: they must either be infinite or closed. A closed finite thermalization surface is possible only in a closed universe with finite (non-eternal) inflation. As Fig. 3 illustrates, thermalization surfaces in an eternally inflating universe extend indefinitely in the τ direction and have, therefore, infinite volumes. It is easily understood that the number of disconnected thermalization surfaces in our double-well model is also infinite. Thermalized regions include inflating islands which in turn include thermalized regions of both types, and so on *ad infinitum*. Regions of the same type may later merge and be, therefore, bounded (in spacetime) by the same thermalization surface. But clearly there is going to be an infinite succession of nested regions of different types which are bounded by disconnected thermalization surfaces.

For an observer in one of the thermalized spacetime regions, the surface Σ_* at the boundary of that region plays the role of the big bang. The natural choice of the time coordinate in the vicinity of that surface is $t = \varphi$, so that the constant- t surfaces are (nearly) surfaces of constant energy density. Since these surfaces are infinite, the observer finds herself in an infinite thermalized universe, which is causally disconnected from the other thermalized regions. The situation here is similar to that in the ‘open-universe’ inflation, where thermalized regions are located in the interiors of expanding bubbles and have the geometry approximating open ($k = -1$) Robertson-Walker universes.

It is now easy to see why the probability distributions obtained using a cutoff at $t = t_c$ are so sensitive to the choice of the time variable t . Any spacelike surface \mathcal{S} can be an equal-time surface $t = t_c$ with an appropriate choice of t . Depending on one’s choice, the surface \mathcal{S} may cross many thermalized regions of different types (e.g., for $t = \tau$), may cross only regions of one type, or may cross no thermalized regions at all (say, for $t = \varphi$ with φ in the slow-roll range). These possibilities are illustrated in Fig. 4 by surfaces $\mathcal{S}_1, \mathcal{S}_2$ and \mathcal{S}_3 , respectively. If, for example, one uses the surface \mathcal{S}_2 as the cutoff surface, one would conclude that all observers will see the same vacuum [the same minimum of $V(\varphi)$] with 100% probability. With a suitable choice of the surface, one can get any result for the relative probability of the two minima.

B. Two-field model

We now consider a two-field model with a potential

$$V(\varphi, \chi) = V_0 \cos^2(\alpha\varphi)[1 + \lambda(1 + \cos\beta\chi) \sin^4\alpha\varphi]. \quad (12)$$

The potential is symmetric with respect to $\chi \rightarrow -\chi$, and we shall not distinguish between the values χ and $-\chi$, so the effective range of the field χ is $0 \leq \chi \leq \pi/\beta$. The maximum of

the potential is at $\varphi = 0$ and the true vacuum is at $\varphi = \pm\eta$. The field χ is massless in the true vacuum, while the mass of φ is χ -dependent,

$$m_\varphi^2(\chi) = 2V_0\alpha^2[1 + \lambda(1 + \cos\beta\chi)]. \quad (13)$$

The expansion rate in the model (12) depends on both φ and χ ,

$$H^2(\varphi, \chi) = \frac{8\pi}{3}V(\varphi, \chi). \quad (14)$$

The quantum and thermalization boundaries, φ_q and φ_* , are also χ -dependent; they are determined from

$$|H'_\varphi(\varphi_q, \chi)| \sim H^2(\varphi_q, \chi), \quad (15)$$

$$|H'_\varphi(\varphi_*, \chi)| \sim 6H(\varphi_*, \chi). \quad (16)$$

An important special case is when H is essentially independent of χ in the quantum regime and near thermalization. Then φ_q and φ_* are also nearly constant. Our model (12) belongs to this class when λ and β are sufficiently small.

For small β and λ , the χ -dependence of the potential is weak and the evolution of φ in the slow-roll regime is essentially the same as in the one-field model (8), with χ remaining nearly constant. Different parts of the universe will thermalize with different values of χ due to quantum fluctuations in the random-walk regime near the top of the potential. This will result in spatial variation of the amplitude of density fluctuations [1],

$$\delta\rho/\rho(\chi) \sim 200m_\varphi(\chi). \quad (17)$$

In the opposite regime, the classical evolution and quantum fluctuations of χ are non-negligible during the slow-roll of φ . In this case, the density fluctuations will not be directly related to the value of χ at thermalization, as in Eq. (17). The quantitative conditions for the two regimes will be specified in Section IV.

In order to make the quantum dispersion of χ during the time of the simulation comparable to the range of χ , we had to use a relatively large value of $\beta = 10$ (see Section V). We used the same values of V_0 and α as before and $\lambda = 0.1$. With these parameters, one finds that φ_q and φ_* are essentially independent of χ and are approximately given by Eqs. (9),(10).

The spacetime structure of the universe in this model is very similar to that in the one-field model (8). There is an infinite number of infinite thermalization surfaces, with the field χ varying continuously along these surfaces. Fig. 5 gives a snapshot of a simulation where different values of χ at thermalization are shown with different shades of grey, from light grey for $\chi = 0$ to dark grey for $\chi = \pi/\beta$. Inflating regions are white as before, and here we do not distinguish between regions thermalizing at $\varphi = +\eta$ and $\varphi = -\eta$, assuming that they have identical physics. A spacetime slice through this simulation is shown in Fig. 6, where now the values of χ are indicated throughout the inflating region using the same shading code, while thermalized regions are white.

Let us now try to understand the gauge dependence of probabilities obtained by a constant- t cutoff in this model. The simple explanation that we gave for the one-field

model, that constant- t surfaces can be chosen so that they cross one type of thermalization surfaces and avoid the other, does not apply here. The field χ takes all its possible values on each thermalization surface Σ_* , and the distributions of χ on different surfaces should be statistically equivalent. However, when we change the time variable, say, from $t = \tau$ to $t = a$, the shape of the cutoff surface $t = t_c$ is also changed, and it is important to note that the direction in which this surface is deformed is correlated with the local value of χ . The scale-factor time a is greater in regions where the expansion rate H is higher, and since the expansion rate is χ -dependent, the cutoff surface deformation will tend to favor regions with χ corresponding to low values of H and will tend to exclude regions where χ corresponds to high values of H . This is the origin of the gauge dependence of the cutoff procedure.

One might have thought that the deformation of the cutoff surface due to the change of the time variable should affect only the boundaries of the thermalized regions included in the calculation of probabilities and should therefore have little effect in the limit $t_c \rightarrow \infty$ when the volume of the thermalized regions gets very large. However, the volume of thermalized regions in an eternally inflating universe grows exponentially with time, and at any time the total thermalized volume is dominated by the newly thermalized regions which stopped inflating within the last few Hubble times.¹ Hence, most of the thermalized volume is always in the vicinity of the cutoff surface $t = t_c$, and it is not surprising that the probability distribution $\mathcal{P}(\chi)$ is sensitive to the choice of the time variable t used to implement the cutoff.

The spacetime structure may be different for other models of eternal inflation, particularly for topological inflation [15] with a different topology. For example, in the case of inflating monopoles one can expect inflating regions to be localized and to be surrounded by thermalized regions. It is conceivable that in this case there is a single connected thermalized region of spacetime which is separated from the inflating regions by a single thermalization surface Σ_* . Despite this possible difference, we still expect that the constant-time cutoff procedure will still give gauge-dependent results, for the same reasons as in the two-field model discussed above.

III. THE PROPOSAL

We now review the resolution of the gauge dependence problem proposed in Ref. [13]. Let us first assume that inflating and thermalized regions of spacetime are separated by a single thermalization surface Σ_* . The problem with the constant-time cutoff procedures is that they cut the surface Σ_* in a biased way, favoring certain values of χ and disfavoring other values. We thus need an unbiasedly selected portion of Σ_* .

It appears that the simplest strategy is to use a “spherical” cutoff. Choose an arbitrary

¹Remember that Figs. 5,6 show the comoving volume distributions of χ . The physical volumes are related to the co-moving volumes by the factor $a^3(\mathbf{x}, t)$, so the volumes thermalizing at later times are exponentially enhanced. Moreover, as Figs. 5,6 indicate, a fixed-time cutoff tends to produce a multitude of disconnected thermalized regions. Their total volume is dominated by small, newly formed regions.

point P on Σ_* . Define a sphere of radius R to include all points Q whose geodesic distance² from P along Σ_* is $d(Q, P) \leq R$. We can use Eq. (1) to evaluate the probability distribution $\mathcal{P}(\chi)$ in a spherical volume of radius R_c and then let $R_c \rightarrow \infty$. If the fields χ_a vary in a finite range, they will run through all of their values many times in a spherical volume of sufficiently large radius. We expect, therefore, that the distribution $\mathcal{P}(\chi)$ will rapidly converge as the cutoff radius R_c is increased. We expect also that the resulting distribution will be independent of the choice of point P which serves as the center of the sphere.

The same procedure can be used for fields with an infinite range of variation, provided that the probability distributions for χ_a are concentrated within a finite range, with a negligible probability of finding χ_a very far away from that range.

Suppose now that there is an infinite number of disconnected thermalization surfaces, as in the two-field model of Section II. We can then pick an arbitrary connected component of Σ_* and apply the spherical cutoff prescription described above. Since the inflationary dynamics of the fields χ_a have a stochastic nature, the distributions of χ_a on different connected components of Σ_* should be statistically equivalent, and the resulting probability distribution $\mathcal{P}(\chi)$ should be the same for all components.

An even more complicated spacetime structure is found in models with a non-vanishing cosmological constant. In such models, regions of true vacuum in the post-inflationary universe may fluctuate back to the quantum diffusion range of the inflaton potential. Every such region will serve as a seed for a new eternally inflating domain whose internal structure will resemble that shown in Fig. 5. Thermalized regions formed in this domain will in turn produce new inflating seeds, etc. [16]. In such a “recycling” universe, there is an infinite number of thermalization surfaces to the future of any given thermalization surface. But once again, we expect them all to be statistically equivalent, so the prescription for probabilities remains the same.

We note that this prescription cannot be applied to models where the potential has a discrete set of minima, as in the double-well model of Section II. We can introduce a discrete variable χ labelling different minima. Each connected component of the thermalization surface Σ_* is then characterized by a single value of χ , and it is clear that the probability distribution for χ cannot be determined by studying one such component.³ This may indicate that no meaningful probability distribution can be defined for a discrete variable in an eternally inflating universe.

Having specified the cutoff procedure, the problem of calculating $\mathcal{P}(\chi)$ can now be split into two parts. The number of galaxies $d\mathcal{N}(\chi)$ in Eq. (1) is proportional to the volume of the comoving regions where χ_a take specified values and to the density of galaxies in those regions. The volumes and the densities can be evaluated at any time. Their product should be independent of the choice of this reference time, as long as we include both galaxies that were formed in the past and those that are going to be formed in the future. It will be convenient to evaluate the volumes and the densities at the time when inflation ends and

²If there is more than one geodesic connecting P and Q , $d(Q, P)$ is defined as the smallest of all the geodesic distances.

³We assume that the discrete vacua cannot be connected by non-inflating domain walls.

vacuum energy thermalizes, that is, on the thermalization surface Σ_* . Then we can write

$$\mathcal{P}(\chi) \propto \nu(\chi)\mathcal{P}_*(\chi). \quad (18)$$

Here, $\mathcal{P}_*(\chi)d^n\chi$ is proportional to the volume of thermalized regions where χ_a take values in the intervals $d\chi_a$, and $\nu(\chi)$ is the number of galaxies that form per unit thermalized volume with cosmological parameters specified by the values of χ_a . The calculation of $\nu(\chi)$ is a standard astrophysical problem which is completely unrelated to the calculation of the volume factor $\mathcal{P}_*(\chi)$. Our focus in this paper will be on the volume factor. In the following sections we shall discuss some methods that can be used to calculate $\mathcal{P}_*(\chi)$.

IV. THE FOKKER-PLANCK EQUATION

A. Derivation of the Fokker-Planck equation

A statistical description of fluctuating quantum fields in an eternally inflating universe can be given in terms of the probability distribution on equal time surfaces, $P(\varphi, \chi, t)$, which satisfies the Fokker-Planck equation. This description was suggested in Ref. [6], where the idea of eternal inflation was first introduced, and was further developed in Refs. [17–20,4,21]. Although this is an elegant formalism, previous attempts to use it for the calculation of probabilities gave ambiguous gauge-dependent answers [4,22,7]. Here we suggest a version of the Fokker-Planck formalism which allows an unambiguous calculation of $\mathcal{P}_*(\chi)$ in a wide class of models.

The idea is that for $\varphi \gg \varphi_q$, when quantum fluctuations of φ (but not necessarily of χ) are negligible compared to its classical motion, the evolution of φ at any given co-moving point is essentially monotonic in proper time and we can use φ as a new time variable, $t = \varphi$. Let us first assume that the χ -dependence of the expansion rate H is insignificant near thermalization, so that φ_* is also nearly independent of χ . Then the thermalization boundary $\varphi = \varphi_*$ is a constant-“time” surface and the probability distribution $\mathcal{P}(\chi)$ is given simply by $P(\varphi_*, \chi)$. We shall now derive the Fokker-Planck equation for $P(\varphi, \chi)$. That equation will be applicable in the regime $\varphi \gg \varphi_q$ where the evolution of φ is essentially classical (but without such restrictions on χ), and will have to be complemented by appropriate boundary conditions (see Section IV, B).

The classical drift velocity of χ in time $t = \varphi$ can be written as

$$v_\chi \equiv \frac{d\chi}{d\varphi} = \frac{\dot{\chi}}{\dot{\varphi}} = \frac{H'_\chi}{H'_\varphi}, \quad (19)$$

where dots indicate derivatives with respect to the proper time τ , $H(\varphi, \chi)$ is given by Eq. (14) and $H'_\chi = \partial H/\partial\chi$, etc. The quantum dispersion during the “time” increment $d\varphi$ is

$$(\delta\chi_q)^2 = \frac{H^3}{4\pi^2}d\tau = -\frac{H^3}{\pi H'_\varphi}d\varphi \equiv 2D(\varphi, \chi)d\varphi, \quad (20)$$

where $D(\varphi, \chi)$ is the diffusion coefficient. Finally, the rate of the cosmological expansion is

$$\frac{1}{a} \frac{\partial a}{\partial \varphi} = \frac{H}{\dot{\varphi}} = -4\pi \frac{H}{H'_\varphi}. \quad (21)$$

The Fokker-Planck (FP) equation for $P(\varphi, \chi)$ can now be written as

$$\frac{\partial P}{\partial \varphi} = \frac{\partial^2}{\partial \chi^2}(DP) - \frac{\partial}{\partial \chi}(v_\chi P) - 4\pi d \frac{H}{H'_\varphi} P, \quad (22)$$

where d is the number of spatial dimensions. The first and second term on the right-hand side of (22) describe the quantum diffusion and the classical drift of χ , respectively, and the last term accounts for the expansion of the universe. Eq. (22) can also be derived directly from the FP equation for the two-field distribution function $P(\varphi, \chi, t)$; this is done in Appendix A. We should note that due to the growth of physical volume, the distribution $P(\varphi, \chi)$, just like $P(\varphi, \chi, t)$, is not normalized. The physical probability distribution for χ is given by $P(\varphi_*, \chi)$ after an appropriate normalization of that function over the range of χ .

Starobinsky has pointed out [17] that the diffusion term of the FP equation suffers from the ambiguity in the ordering of non-commuting factors $\partial/\partial\chi$ and $D(\varphi, \chi)$. For example, one could write this term as

$$\frac{\partial}{\partial \chi} \left[D^{1/2+\gamma} \frac{\partial}{\partial \chi} \left(D^{1/2-\gamma} P \right) \right]. \quad (23)$$

However, it has been recently shown [23] that the so-called Ito factor ordering, $\gamma = -1/2$, has significant advantages compared to other choices. Hence, we used $\gamma = -1/2$ in Eq. (22).

It is also possible to relax the assumption that the thermalization surface $\phi = \phi_*$ is independent of χ . Usually the endpoint ϕ_* is defined only approximately and one could redefine its exact position (within the range where fluctuations of both χ and ϕ are negligible) to remove the dependence of ϕ_* on χ , without changing the physical results. In case such redefinition is impossible, the formalism can be extended to give the distribution of χ along an arbitrary boundary line specified by a function $\phi_*(\chi)$. To implement this, one formally puts the diffusion coefficient $D(\phi, \chi)$ and the drift velocity v_χ to zero everywhere in the domain $\phi > \phi_*(\chi)$ and solves the modified FP equation in the entire range of ϕ and χ up to a suitable value $\phi = \phi_{\max}$ which should lie beyond the boundary $\phi_*(\chi)$ for all χ . The solution of the new FP equation adequately describes fluctuations of χ up to the boundary, while beyond the boundary the distribution is kept unchanged for a given χ . The restriction of this solution to $\phi = \phi_{\max}$ (clearly independent of the choice of ϕ_{\max}) gives the desired probability distribution $\mathcal{P}_*(\chi)$. We shall therefore assume below that the boundary ϕ_* is independent of χ .

B. Initial conditions

To solve the FP equation (22) we have to specify the initial distribution $P(\varphi_0, \chi)$ at some $\varphi = \varphi_0$ in the deterministic slow-roll range, $\varphi_q(\chi) \ll \varphi_0 < \varphi_*(\chi)$. We do not know how to do this in the general case. However, a simple initial distribution can be specified in models where the potential $V(\varphi, \chi)$ is very symmetric near the top, so that it is essentially independent of χ in the interval $0 \leq \varphi < \varphi_1$ which includes the diffusion range and part of the slow-roll range ($\varphi_q \ll \varphi_1 < \varphi_*$). We can then choose φ_0 to be in the part of the slow-roll range where the potential is still symmetric ($\varphi_q \ll \varphi_0 < \varphi_1$).

Let us consider the (spacelike) surface $\Sigma_0 : \varphi(x) = \varphi_0$. In the slow-roll regime φ rolls from smaller to larger values, and thus the values of φ in the past of Σ_0 are in the range

$\varphi_q \lesssim \varphi < \varphi_0$, and prior to that in the diffusion range $-\varphi_q \lesssim \varphi \lesssim \varphi_q$. In both of these ranges the potential is nearly independent of χ , and therefore we expect the distribution $P(\varphi_0, \chi)$ on Σ_0 to be flat,

$$P(\varphi_0, \chi) = \text{const}, \quad (24)$$

with all values of χ equally probable.

We shall now specify the conditions of applicability of the distribution (24). Suppose the potential $V(\varphi, \chi)$ can be represented as

$$V(\varphi, \chi) = U(\varphi) + \mathcal{V}(\varphi, \chi) \quad (25)$$

with $\mathcal{V} \ll U$. The expansion rate can be written as

$$H(\varphi, \chi) = H(\varphi) + \delta H(\varphi, \chi), \quad (26)$$

where

$$\delta H(\varphi, \chi) \approx 4\pi\mathcal{V}(\varphi, \chi)/3H(\varphi). \quad (27)$$

Let us consider the physical processes affecting the distribution of χ and their characteristic timescales. The χ -dependent correction to the expansion rate (27) will tend to distort the distribution, producing a peak at the maximum of $\mathcal{V}(\varphi, \chi)$ where the expansion rate is the highest. This differential expansion becomes important on a timescale τ_{de} such that $\delta H\tau_{de} \sim 1$,

$$\tau_{de} \sim 1/\delta H. \quad (28)$$

On the other hand, the classical force will tend to drive χ to the minimum of $\mathcal{V}(\varphi, \chi)$ on a timescale

$$\tau_c \sim \frac{\Delta\chi}{v_c} \sim 4\pi \frac{\Delta\chi^2}{\delta H}, \quad (29)$$

where we have used $v_c = -\delta H'_\chi/4\pi \sim \delta H/4\pi\Delta\chi$ for the classical drift velocity.⁴ Finally, the quantum diffusion of χ will tend to keep the distribution flat. The typical variation of χ due to the quantum random walk in a proper time interval τ is $(\Delta\chi)^2 \sim (H^3/4\pi^2)\tau$. The time τ_q it takes χ to spread over its entire range $\Delta\chi$ is

$$\tau_q \sim \Delta\chi^2/H^3. \quad (30)$$

The effect of randomization due to diffusion will prevail over the differential expansion and classical drift, provided that

$$\tau_q \ll \tau_c, \tau_{de}, \quad (31)$$

⁴Note that v_c is different from v_χ in Eq. (8) because the velocity v_χ is defined with respect to “time” φ , while v_c is defined with respect to the proper time.

or,

$$\frac{\Delta_\chi^2 \delta H}{H^3} \ll 1, \quad \frac{1}{4\pi} \frac{\delta H}{H^3} \ll 1. \quad (32)$$

If conditions (32) are satisfied at $\varphi \lesssim \varphi_q$, then we expect that $P(\varphi_q, \chi) \approx \text{const}$ at the onset of the slow roll. At $\varphi \gg \varphi_q$, the inflaton φ grows monotonically with time, causing an evolution of the expansion rate H and of the potential \mathcal{V} . This introduces two additional timescales

$$\tau_H \sim H/\dot{H} \sim 4\pi H/H'_\varphi{}^2 \quad (33)$$

and

$$\tau_{\mathcal{V}} \sim \mathcal{V}/\dot{\mathcal{V}} \sim \frac{4\pi}{H'_\varphi} \frac{\delta H}{\delta H'_\varphi}. \quad (34)$$

If both of these times are large compared to τ_q , then the flat distribution of χ extends into the slow roll regime for as long as τ_q remains the smallest of all relevant times. In fact, the evolution of H and \mathcal{V} does not by itself distort the flat distribution of χ , and one can expect that this distribution persists as long as the conditions (32) are satisfied, even if τ_q gets larger than τ_H or $\tau_{\mathcal{V}}$.

Another interesting case where the probability distribution for χ can be specified is when τ_c and τ_q are small compared to all other relevant timescales,

$$\tau_c, \tau_q \ll \tau_{de}, \tau_H, \tau_{\mathcal{V}}. \quad (35)$$

Then the distribution $P(\varphi, \chi)$ is determined by a statistical equilibrium between the quantum diffusion and the classical drift. This equilibrium distribution is given by [24]

$$P_{eq}(\varphi, \chi) \propto \exp\left(-\frac{8\pi^2 \mathcal{V}(\varphi, \chi)}{3H^4(\varphi)}\right). \quad (36)$$

It is an approximate solution of Eq. (22) when the φ -dependence of D and v_χ can be disregarded and the last term in (22) can be dropped. We note that it follows from Eqs. (29),(30) and (27) that

$$\frac{8\pi^2 \mathcal{V}}{3H^4} \sim 8\pi^2 \frac{\tau_q}{\tau_c}. \quad (37)$$

Hence, for $8\pi^2 \tau_q \ll \tau_c$ the distribution (36) is nearly flat, as expected. In the opposite limit, $\tau_c \ll \tau_q$, the distribution is strongly peaked at the minimum of $\mathcal{V}(\varphi, \chi)$. If the conditions of equilibrium (35) are satisfied at some φ_0 in the range $\varphi_q \ll \varphi_0 < \varphi_*$, we can use $P_{eq}(\varphi_0, \chi)$ as the initial condition for the FP equation at $\varphi = \varphi_0$.

C. Some examples

We shall now give some examples of numerical and analytic solutions of the FP equation (22) for the two-field model (12). In this model $U(\varphi) = V_0 \cos^2(\alpha\varphi)$, $\mathcal{V}(\varphi, \chi) = \lambda V_0 \cos^2(\alpha\varphi) \sin^4(\alpha\varphi) (1 + \cos \beta\chi)$, $\Delta_\chi = \pi/\beta$, and the conditions (32) which ensure a flat distribution at the onset of the slow roll take the form

$$\lambda H_0^2 / 8\pi\alpha^4 \ll 1, \quad (\pi/\beta)^2 (\lambda H_0^2 / \alpha^4) \ll 1. \quad (38)$$

Here we have used $\varphi \sim \varphi_q \sim H_0/\alpha^2$.

In our first example we used

$$\alpha = 0.1, \quad \beta = 0.1, \quad \lambda = 0.01, \quad H_0 = 10^{-6} \quad (39)$$

and the initial condition $P = \text{const}$ at $\varphi_0 = 10^{-3}$ (which is above $\varphi_q \sim 10^{-4}$). These values of the parameters could occur in a realistic inflationary model: Eqs. (13) and (17) give $m_\phi \sim 5 \times 10^{-7}$ and $\delta\rho/\rho \sim 10^{-5}$. The characteristic times for the parameters (39) are plotted in Fig. 7 as functions of φ . We see that the conditions (31) are initially satisfied, and thus we are justified to use a flat distribution as the initial condition. The result of a numerical integration of Eq. (22) is shown in Fig. 8. At $\varphi = \varphi_*$, the distribution is peaked at $\chi = 0$, indicating that the effect of differential expansion was more important than that of classical drift and of diffusion. This is not surprising, since $\tau_{de} \ll \tau_q, \tau_c$ in most of the slow roll range.

The classical variation of χ during the slow roll of φ from some $\varphi_0 > \varphi_q$ to φ_* is given by

$$\delta\chi_c = \int_{\varphi_0}^{\varphi_*} \frac{\mathcal{V}'_\chi}{U'_\varphi} d\varphi \sim \lambda\beta/\alpha^2 \quad (40)$$

and is essentially independent of φ_0 . Similarly, the variation of χ due to quantum fluctuations is

$$(\delta\chi_q)^2 = \int \frac{H^3}{4\pi^2} d\tau = -\frac{1}{\pi} \int_{\varphi_0}^{\varphi_*} \frac{H^3}{H'_\varphi} d\varphi \approx \frac{H_0^2}{\pi\alpha^2} \ln \frac{\sin(\alpha\varphi_*)}{\sin(\alpha\varphi_0)}, \quad (41)$$

with only a logarithmic dependence on φ_0 . For the parameter values in our example, both $\delta\chi_c$ and $\delta\chi_q$ are small compared to the range of χ , $\Delta_\chi = \pi/\beta$, and thus χ remains nearly constant during the slow roll.

When both diffusion and classical drift are negligible, the first two terms on the right-hand side of the FP equation (22) can be dropped, and the solution of (22) is

$$P(\varphi_*, \chi) \propto \exp\left(-4\pi d \int_{\varphi_0}^{\varphi_*} \frac{H(\varphi, \chi)}{H'_\varphi(\varphi, \chi)} d\varphi\right) = e^{N(\chi)d}. \quad (42)$$

Here,

$$N(\chi) = \int H d\tau = -4\pi \int_{\varphi_0}^{\varphi_*} \frac{H}{H'_\varphi} d\varphi \approx N_0 + \frac{2\pi\lambda}{\alpha^2} \cos(\beta\chi) \quad (43)$$

is the number of inflationary e-foldings between φ_0 and φ_* , N_0 is the number of e-foldings in the χ -independent case ($\lambda = 0$), and we have used $\sin(\alpha\varphi_*) \approx 1$, which is valid for $\alpha \lesssim 1$ [see Eq. (10)]. Eq. (42) has a simple interpretation [13]: if χ remains nearly constant, then the probability distributions for χ at $\varphi = \varphi_0$ and $\varphi = \varphi_*$ are related simply by the volume expansion factor e^{N_d} . Our numerical solution (which was done for $d = 3$) agrees with the analytic solution (42) within 10%.

Our second example is

$$\alpha = 0.01, \quad \beta = 10^4, \quad \lambda = 10^{-8}, \quad H_0 = 10^{-4} \quad (44)$$

with a flat initial condition at $\varphi = 10$. The characteristic timescales for this case are plotted in Fig. 9 and the numerical solution of the equation is shown in Fig. 10. In this example, τ_q is initially much smaller than all other characteristic times, and thus the use of the flat initial condition is justified. The distribution develops a peak at $\chi = \pi/\beta$ at “time” $\varphi \sim 60$, when $8\pi^2\tau_q/\tau_c \sim 1$, as expected [see Eq.(37)]. τ_c and τ_q remain smaller than other characteristic times throughout the slow roll period, so one expects that the equilibrium distribution (36) should be an approximate solution of the FP equation (22). We have verified that this is indeed the case, with a very good accuracy. The two distributions begin to diverge as we approach thermalization ($\varphi \sim 140$), presumably because τ_ν becomes comparable to τ_c and τ_q . However, even at $\varphi = 140$ the equilibrium distribution is accurate within $\sim 5\%$. We had to terminate the numerical solution at $\varphi = 140$, somewhat short of $\varphi_* \approx 157$, because the peak of the distribution was getting too narrow.

Finally, we present a numerical solution of Eq. (22) for the parameters we used in the simulations:

$$\alpha = 1, \quad \beta = 10, \quad \lambda = 0.1, \quad H_0 = 0.63. \quad (45)$$

with a flat initial condition at $\varphi_0 = 0.8$. The simulations were performed in $(1 + 1)$ dimensions, so we used $d = 1$. (This choice of parameters was dictated by computational constraints; see Section V). The characteristic timescales for this example are plotted in Fig. 11 and the solution is shown in Fig. 12. Once again, we see that initially τ_q is smaller than all other timescales, and thus our choice of the initial condition is justified. But towards the end of the slow roll, τ_c , τ_{de} and τ_H become comparable to τ_q , within an order of magnitude. So in this example the shape of the final distribution at $\varphi = \varphi_*$ is hard to predict without a numerical solution of the FP equation.

For the parameter values (45) we have $\varphi_q \sim 0.63$, which is close to the initial value $\varphi_0 = 0.8$. Strictly speaking, φ cannot be used as a time variable in such proximity of φ_q . However, our solution of the FP equation is in a good agreement with the distribution $P(\varphi, \chi)$ obtained from numerical simulations (see Section V). This indicates that our method is robust and gives a reasonable accuracy even for $\varphi_0 \sim \varphi_q$.

V. NUMERICAL SIMULATIONS

The most direct approach to the calculation of $\mathcal{P}_*(\chi)$ is to use a numerical simulation of eternally inflating spacetime. The first simulation of this sort [14] was performed on a square lattice representing a comoving region of initial size H^{-1} in a $(2 + 1)$ -dimensional

universe. The initial value of the inflaton φ was set to $\varphi = 0$ at all points of the lattice. The potential was assumed to be very flat in the whole range $|\varphi| < \varphi_*$, so that $H \approx \text{const}$ throughout the inflating region. Then there is no classical slow roll, and the evolution of φ is driven entirely by quantum fluctuations. The fluctuations were simulated by adding random increments to φ independently in each horizon-size region. After each two-folding of expansion, square regions which had physical size H^{-1} at the previous step were subdivided into four smaller squares and a fluctuation, drawn from a Gaussian distribution of width $(H/2\pi)(\ln 2)^{1/2}$, was added to φ in each of these squares. Whenever $|\varphi|$ exceeded φ_* , the corresponding cell was marked as thermalized.

Linde, Linde and Mezhlumian [25,4] developed more realistic simulations which allow for the slow roll of φ . They performed simulations of inflating domain walls and vortices in $(2 + 1)$ dimensions. The classical change of φ in a small proper time increment $\Delta\tau$ was taken as [see Eq. (5)]

$$\Delta\varphi = -\frac{V'(\varphi)}{3H}\Delta\tau \quad (46)$$

and quantum fluctuations were represented by sinusoidal waves

$$\delta\varphi(\mathbf{x}) = \frac{H}{\sqrt{2\pi}}\sqrt{H\Delta\tau}\sin\left(He^{H\tau}(\mathbf{n}\cdot\mathbf{x} + \alpha)\right) \quad (47)$$

of wavelength comparable to the horizon, $\ell = 2\pi/H$. A phase α and a unit two-dimensional vector \mathbf{n} were chosen at random at each step of the simulation. The expansion rate H was still treated as a constant.

LLM have also performed $(1 + 1)$ and $(2 + 1)$ -dimensional simulations in which they included the effect of variation of the expansion rate H in space and time [4]. In $(1 + 1)$ dimensions they still used the sinusoidal *ansatz* for the fluctuations, but now the amplitude and the wavelength of the sine depended on the local value of $H(x, \tau)$. In $(2 + 1)$ dimensions with a variable $H(x, \tau)$ this *ansatz* could not be used and LLM represented the fluctuations by wavelets.

An advantage of using the sine waves is that they give a continuous variation of φ , in contrast to the discontinuous jumps along the boundaries of the squares in the method of Ref. [14]. However, use of the sine functions presents two problems. Firstly, the sine waves introduce unphysical correlations between the values of $\delta\varphi$ at points separated by large distances⁵. In this respect the simulation of Ref. [14], which treated $\delta\varphi$ in neighboring horizon regions as completely uncorrelated, was more realistic. We note, however, that the calculation of probability distribution will be unaffected by these extra correlations, provided that the values of χ are sufficiently well sampled throughout the volume. Also, the wavelet representation of fluctuations, as used by LLM in $2 + 1$ -dimensional simulations, eliminates correlations at distances beyond the wavelet size (which was taken to be larger than the horizon size in LLM).

⁵The unphysically large long-distance correlations resulting from Eq. (47) disappear only in the limit of $\Delta\tau \rightarrow 0$. These issues will be addressed in more detail in Ref. [26].

Secondly, the fluctuation amplitude computed with the sine wave *ansatz* is strictly bounded from above by the value it takes when the sine function in Eq. (47) is equal to one. In reality, the amplitude of the fluctuations is a Gaussian variable, and large values of $\delta\varphi$ are suppressed but not strictly forbidden. LLM have dealt with this problem by using a small timestep ($\Delta\tau \ll H^{-1}$), effectively using a superposition of many sine waves with random phases in each Hubble time. This approximates the desired Gaussian distribution significantly better than a single sine wave (although it does not eliminate unphysical correlations at large distances).

Motivated by these considerations, we have attempted to develop simulations that do not suffer from these problems, as described in Sections V A.

Numerical simulations of eternal inflation encounter significant computational constraints, and we were able to perform simulations only for a restricted range of parameter values. Suppose we do the simulation starting with $\varphi = 0$ in a horizon-size region, $l_0 = H_0^{-1}$. After N e-foldings of expansion, the size of our comoving region is $l = H_0^{-1}e^N$. The simulation has to stop when there are still a few grid points per horizon, and realistically the total number of points cannot exceed $\mathcal{N}_{max} \sim 10^7$. Then, in a $(d+1)$ -dimensional simulation, the number of inflationary e-foldings is

$$N \lesssim d^{-1} \ln \mathcal{N}_{max} + \ln(H_0/H_*) \sim 16/d, \quad (48)$$

where we have assumed that $\ln(H_0/H_*) \sim \ln(6/\alpha) \lesssim 16/d$.

The number of inflationary e-foldings in the slow-roll range $\varphi_q < \varphi < \varphi_*$ is

$$N = -4\pi \int_{\varphi_q}^{\varphi_*} \frac{H}{H'_\varphi} d\varphi \approx \frac{4\pi}{\alpha^2} \ln \frac{\sin(\alpha\varphi_*)}{\sin(\alpha\varphi_q)} \approx \frac{4\pi}{\alpha^2} \ln \frac{\alpha}{H_0}, \quad (49)$$

and it follows from Eq. (48) that we need $\alpha \gtrsim 1$. On the other hand, α is bounded from above by $\alpha \lesssim 1$, since otherwise there is no eternal inflation in this model. We used the value $\alpha = 1$.

The dependence of N on H_0 is only logarithmic, but still the number of e-foldings is too large for small values of H_0 . We used $H_0 = 0.63$ (which corresponds to $V_0 = 0.05$). This value of H_0 is dangerously close to the Planck scale, but here we disregard all complications of quantum gravity. (Our choice of parameters in these simulations was dictated by the computational constraints, and we made no attempt to make this choice realistic.)

In two-field simulations, the dispersion of χ due to quantum fluctuations is

$$\delta\chi_q \sim \frac{H_0}{2\pi} N^{1/2} \approx 0.6 \frac{H}{\sqrt{d}}. \quad (50)$$

In order to have a representative simulation, we require that χ should spread through its entire range (π/β) by the end of the simulation. This implies $\delta\chi_q \gtrsim \pi/\beta$, or $\beta \gtrsim 5d^{1/2}H^{-1}$. In our simulations we used $d = 1$, $\beta = 10$.

A. Comoving space simulations

The first series of simulations described the spacetime in co-moving coordinates. The simulation was performed on a co-moving grid of points in either 2 or 1-dimensional space.

Both the one-field and the two-field models were simulated. Initially the field values were taken constant throughout the grid, with $\varphi = 0$. At each timestep, the fields were incremented by the classical evolution term $\Delta\varphi$ from Eq. (46) and by the corresponding quantum fluctuation $\delta\varphi(\mathbf{x})$. The evolution of the field χ in the two-field model was computed in the same manner. The simulation was continued until the physical distance between adjacent grid points grew larger than the horizon size.⁶ The expansion factor was calculated for each point to determine the probability distribution of χ weighted by the physical volume.

Instead of taking the sine waves, we used for $\delta\varphi(\mathbf{x})$ true Gaussian random fields with an appropriate correlation function. To obtain the increments for the grid points at each step, one only needs to generate a set of Gaussian variables $\delta\varphi(\mathbf{x}_i)$ with zero mean and correlation matrix

$$\langle\delta\varphi(\mathbf{x}_i)\delta\varphi(\mathbf{x}_j)\rangle\equiv C_{ij}=C(d(\mathbf{x}_i,\mathbf{x}_j)),\quad(51)$$

where d is the geodesic distance between points $\mathbf{x}_i, \mathbf{x}_j$ calculated using the known scale factors at intermediate points. Given the symmetric and positive-definite correlation matrix C_{ij} , one can compute its Cholesky decomposition $C = LL^T$ where L is a lower triangular matrix (see e.g. Ref. [27] for a numerical method), and the required vector of random increments is then obtained as

$$\delta\varphi(\mathbf{x}_i)=L_i^j u_j\quad(52)$$

where u is a vector of uncorrelated random numbers with normal distribution. The correlation function $C(r)$ decays rapidly over the distance of a few horizon sizes and was taken to be zero at distances larger than $2H^{-1}$ to simplify calculations.

We have performed simulations for the double-well model (8) and the two-field model (12). Momentary snapshots and spacetime slices of some of these simulations are shown in Section II. A more systematic investigation of the spacetime structure of eternally inflating universes, based on numerical simulations of this sort, will be given in a separate publication.

B. Physical space simulations

In the second series of simulations we have investigated the thermalization surface of the two-field model of Eq. (12) with the parameter values (45) in $(1+1)$ dimensions. We have already discussed the spacetime structure of the universe in this model (Section IIB). As illustrated in Fig. 6, the universe contains an infinite number of disconnected, infinite, spacelike thermalization lines (thermalization surfaces are lines in a $(1+1)$ -dimensional simulation). In order to implement our prescription for the calculation of probabilities, we have to choose one of these lines and calculate $\mathcal{P}_*(\chi)\propto dl/d\chi$ on a large segment of that

⁶In the $(2+1)$ -dimensional case, we extended the simulations somewhat beyond this point and allowed the separation of adjacent grid points to exceed the horizon in the inflating regions with φ near the top of the potential. This should not have had any effect on the thermalized regions shown in Figures 2 and 5.

line. Here, $d\ell$ is the length of all parts of the segment where χ takes values in the interval $d\chi$. A segment of length $2R$ is a one-dimensional analogue of a sphere of radius R . The probability distribution is obtained in the limit of large R , so we used the whole length of the thermalization line that we were able to generate.

The simulation space is a line of gridpoints, each carrying a value of φ and χ ; initially the values of the fields are set constant everywhere. At every timestep, the fields are evolved by adding the classical drift $\Delta\varphi$ and the quantum fluctuation $\delta\varphi(x)$ generated from Eq. (47) (we chose this over the more precise Eq. (52) for reasons of computational feasibility) in which the sine wave was multiplied by a random factor M ,

$$\delta\varphi(\mathbf{x}) = M \frac{H}{\sqrt{2\pi}} \sqrt{H\Delta\tau} \sin\left(He^{H\tau}(\mathbf{n} \cdot \mathbf{x} + \alpha)\right). \quad (53)$$

It can be verified that if α is uniform in $[0, 2\pi]$ and M has the standard χ^2 distribution with two degrees of freedom, then $M \sin \alpha$ has normal distribution. This modification of Eq. (47) circumvents the problem we mentioned above with the unphysical distribution of the fluctuation amplitude resulting from a fixed-amplitude sine wave.

The local expansion factor is also computed at each point. Due to the one-dimensional geometry of the simulation space, it is possible to maintain an (approximately) constant number of points per physical horizon size by inserting new grid points as necessary at each step. Thus we obtain a connected piece of the thermalization line in *physical* (instead of co-moving) coordinates.

Since the calculation involves only a single thermalization line, one can save a great deal of memory and computer time by discarding parts of the simulation that do not affect that particular line. At any given moment the universe in the simulation consists of thermalized regions of two types (corresponding to $\varphi = \pm\eta$) separated by inflating regions. Suppose we have chosen a plus-region (with $\varphi = +\eta$) for the calculation of $\mathcal{P}_*(\chi)$. This region will never merge with any of the minus-regions, so we can safely discard the nearest minus-regions on both sides and everything beyond them. New minus-regions can later be formed in the remaining part of the simulation, and we can discard them and everything beyond them again. A greater efficiency is achieved by discarding the nearest thermalized regions regardless of their type, so the simulation includes only one thermalized region and two adjacent inflating regions. Once again, the procedure is repeated whenever new thermalized regions are formed. If the discarded nearest neighbors were plus-regions, they can later merge with our region of choice, in which case the simulation will terminate prematurely. This can be fixed by going back to the moment when the merged neighboring region was discarded and performing the simulation for that region from that time on. The resulting thermalization line is then attached to the line obtained for the initial region. We can make an arbitrary number of such attachments to generate a thermalization line of any desired length. We used this attachment procedure in our simulations.

Fig. 13 shows the probability distributions we obtained for two different thermalization lines in our simulations. As expected, the two distributions are very similar. Also shown is the distribution we obtained by solving the Fokker-Planck equation in Section IV C. It agrees with the simulation-based distributions with an accuracy of 4% .

VI. CONCLUSIONS

In this paper we analyzed the origin of the gauge dependence of probability distributions for observables in models of eternal inflation. We reviewed the resolution of this problem proposed in Ref. [13], gave a more precise formulation of this proposal and used it to develop two methods for calculating probabilities.

The root of the problem is that an eternally inflating universe contains an infinite number of observers (galaxies), and one needs to introduce some cutoff procedure in order to calculate probabilities. The proposed procedure can be summarized as follows. Pick an arbitrary galaxy \mathcal{G} at an arbitrary moment in its history; this defines a point in spacetime. Consider the hypersurface of constant energy density Σ passing through that point. Define a sphere of radius R to include all points whose geodesic distance from \mathcal{G} along Σ is less than R . The proposal is to evaluate the probability distribution $P(\chi)$ based on galaxies formed within the co-moving region defined by a sphere of radius R_c and then let $R_c \rightarrow \infty$. The surface Σ is an infinite spacelike surface, and the distribution of the fields χ_a on this surface is statistically homogeneous on large scales. One expects, therefore, that the resulting probability distribution $P(\chi)$ will be independent of the choice of the “central” galaxy \mathcal{G} and that it will rapidly converge once the cutoff radius R_c becomes larger than the characteristic scale ξ of variation of the fields χ_a on Σ .

One argument in favor of this proposal is that it satisfies the “correspondence principle” with models of finite inflation, where the definition of probabilities is unambiguous. In such models, the total number of galaxies in the universe is finite, and all galaxies should in principle be included in the calculation of $P(\chi)$. However, a spherical cutoff with $R_c \gg \xi$ should give a distribution very close to that obtained using the complete set of galaxies.

We performed numerical simulations of eternal inflation in a two-field model (12) and showed how the spherical cutoff can be implemented to calculate the probability distribution $P(\chi)$ numerically. Due to significant computational constraints, we were able to perform simulations only for a rather restricted set of parameter values.

An alternative approach, which does not suffer from these restrictions, is to calculate $P(\chi)$ by solving the Fokker-Planck equation with the inflaton field φ playing the role of time. This form of the FP equation is valid only in the slow-roll range, $\varphi_q \lesssim \varphi \lesssim \varphi_*$, and the method can be used only in cases where one can specify the initial distribution $P(\varphi_0, \chi)$ at some $\varphi_0 \gtrsim \varphi_q$. We have shown in Section IV that this can be done in a reasonably wide class of models. In more general models, one may have to do numerical simulations in the quantum diffusion regime in order to determine the initial conditions for the FP equation in the slow-roll regime.

We have indicated some cases in which the FP equation can be approximately solved analytically. In one of these cases, when the fields χ_a remain nearly constant during the slow roll of φ , the resulting distribution agrees with that obtained in [13]. We obtained a numerical solution of the FP equation for the parameter values used in our simulations and verified that the probability distribution $P(\chi)$ obtained in this way agrees with the distribution calculated directly from the simulations.

The approach we developed in this paper can be extended to models of “chaotic” inflation, where the inflaton potential rises to super-Planckian values. However, in such models one has to deal with the uncertainties associated with Planck physics. In particular, one has to

impose some boundary condition for the FP equation at the ‘‘Planck boundary’’ $\varphi = \varphi_p$, where $V(\varphi_p) \sim 1$.

Perhaps the most important application of our approach would be a probabilistic analysis of the density perturbation spectra. As we emphasized in the Introduction, this problem arises in practically all inflationary models, with or without the additional fields χ_a . A brief discussion of this issue can be found in Ref. [13] where it was argued that the present approach should give essentially the same results as the standard calculations [9]. A more detailed analysis will be given elsewhere.

Our prescription for calculating probabilities cannot be applied to models where χ is a discrete variable. In such models, different values of χ are taken in different, causally disconnected thermalized regions. The spherical cutoff prescription involves only a single thermalized region, and it is clear that it cannot be used to determine the probability distribution in this case. One can take this as indicating that no probability distribution for a discrete variable can be meaningfully defined in an eternally inflating universe. Alternatively, one could try to introduce some other cutoff prescription to be applied specifically in the case of a discrete variable. It is possible that some version of the ϵ -prescription of Ref. [10] could be used for this purpose. This issue requires further investigation.

VII. ACKNOWLEDGMENTS

We are grateful to Jaume Garriga, Andrei Linde and Ken Olum for their comments on the manuscript. The work of A.V. was supported in part by the National Science Foundation. S.W. was supported by PPARC rolling grant GR/L21488.

APPENDIX A: DERIVATION OF THE REDUCED FOKKER-PLANCK EQUATION IN THE LIMIT OF NEGLIGIBLE DIFFUSION

We start from the usual time-dependent FP equation in two dimensions (ϕ, χ) for the co-moving probability distribution $P(t, \phi, \chi)$, under assumption that diffusion in ϕ direction is negligible and using the Ito factor ordering:

$$\partial_t P = \partial_\chi^2 (\tilde{D}(\phi, \chi) P) - \partial_\chi (\tilde{v}_\chi P) - \partial_\phi (\tilde{v}_\phi P). \quad (\text{A1})$$

Here \tilde{v}_ϕ and \tilde{v}_χ are the usual (both ϕ and χ -dependent) drift coefficients,

$$\tilde{v}_\phi = -\frac{1}{4\pi} \partial_\phi H, \quad \tilde{v}_\chi = -\frac{1}{4\pi} \partial_\chi H, \quad (\text{A2})$$

and the diffusion coefficient is $\tilde{D} = H^3/8\pi^2$. The diffusion is bounded by the line $\phi = \phi_*$ which is the absorbing boundary (due to thermalization). No other exit boundaries are present.

First we consider the probability density $P_e(t; \phi, \chi; \phi_*, \chi_*)$ to exit at a particular time t through the neighborhood of a particular point χ_* along the line $\phi = \phi_*$, given that we started at $t = 0$ at a given point (ϕ, χ) . Obtaining the distribution $P_e(t; \dots)$ is a standard problem in the theory of stochastic processes [28]; once we know $P_e(t; \dots)$, we can integrate

it over time until $t = \infty$ and obtain the total probability to thermalize in the neighborhood of χ_* .

According to the standard theory, we can find the *generating function* $g(s; \dots)$ for the distribution $P_e(t; \dots)$, defined as

$$g(s; \phi, \chi; \phi_*, \chi_*) \equiv \int_0^\infty e^{-st} P_e(t; \phi, \chi; \phi_*, \chi_*) dt \quad (\text{A3})$$

because it turns out that g is the solution of the “backward” or adjoint diffusion equation

$$\tilde{D}(\phi, \chi) \partial_\chi^2 g + \tilde{v}_\chi \partial_\chi g + \tilde{v}_\phi \partial_\phi g = sg \quad (\text{A4})$$

with boundary condition at $\phi = \phi_*$ given by

$$g(s; \phi_*, \chi; \phi_*, \chi_*) = \delta(\chi - \chi_*). \quad (\text{A5})$$

This boundary condition makes the function vanish everywhere on the exit boundary except at the point χ_* where we want to find the exit probability. It is seen from Eq. (A3) that the total probability of exit at any time, i.e. the integral of P_e through all t , is equal to the value of g at $s = 0$. This value $g(s = 0; \phi, \chi; \phi_*, \chi_*) \equiv g_0$ is then interpreted as the probability that the diffusion process finishes at $\chi = \chi_*$ if it started at (ϕ, χ) . The boundary condition Eq. (A5) means that if we already started at the boundary but at a different χ , then the probability to exit at the chosen value $\chi = \chi_*$ is zero. The equation for g_0 is

$$\tilde{D}(\phi, \chi) \partial_\chi^2 g_0 + \tilde{v}_\chi \partial_\chi g_0 = -\tilde{v}_\phi \partial_\phi g_0. \quad (\text{A6})$$

This is formally the same as the backward Fokker-Planck equation for a one-dimensional diffusion process with ϕ playing the role of time, where $g_0(\phi, \chi; \phi_*, \chi_*)$ is interpreted as the probability of finishing at $\chi = \chi_*$ at the final “time” $\phi = \phi_*$ if started at (ϕ, χ) . The boundary conditions (A5) correspond exactly to that interpretation. The drift and diffusion coefficients become

$$v_\chi \equiv -\frac{\tilde{v}_\chi}{\tilde{v}_\phi}, \quad D \equiv -\frac{\tilde{D}}{\tilde{v}_\phi} \quad (\text{A7})$$

in agreement with Eqs. (19)–(20). The equation adjoint to Eq. (A6) is therefore interpreted as the diffusion equation for the “time”-dependent probability distribution $P(\phi, \chi; \chi_0)$, with ϕ as “time” and the new kinetic coefficients,

$$\partial_\phi P = \partial_\chi^2 (DP) - \partial_\chi (v_\chi P). \quad (\text{A8})$$

The equations for the physical volume distribution are derived in the same manner and differ from Eqs. (A1)–(A6) only by the addition of the growth term $3HP$ or $3Hg$ as appropriate, and the corresponding growth term in Eq. (A8) is similarly obtained as $-3HP/\tilde{v}_\phi$. We therefore arrive at Eq. (22).

REFERENCES

- [1] For a review of inflation, see, e.g., A.D. Linde, *Particle Physics and Inflationary Cosmology* (Harwood Academic, Chur, Switzerland, 1990); K.A. Olive, Phys. Rep. **190**, 307 (1990).
- [2] A. Vilenkin, Phys. Rev. Lett. **74**, 846 (1995).
- [3] Related ideas have been discussed by B. Carter [unpublished], J. Leslie [Mind **101.403**, 521 (1992)], J.R. Gott [Nature **363**, 315 (1993)], A. Albrecht [in *Lecture Notes in Physics*, Springer-Verlag, Berlin, 1995], and A.D. Linde *et. al.* [4,5].
- [4] A. D. Linde, D. A. Linde, and A. Mezhlumian, Phys. Rev. **D49**, 1783 (1994).
- [5] J. Garcia-Bellido, A.D. Linde and D.A. Linde, Phys. Rev. **D50**, 730 (1994); J. Garcia-Bellido and A.D. Linde, Phys. Rev. **D51**, 429 (1995)
- [6] A. Vilenkin, Phys. Rev. **D27**, 2848 (1983).
- [7] A. D. Linde, Phys. Lett. **B175**, 395 (1986).
- [8] A. D. Linde, D. A. Linde, and A. Mezhlumian, Phys. Lett. **B345**, 203 (1995); Phys. Rev. **D54**, 2504 (1996).
- [9] For a review of density fluctuations in inflationary scenarios, see, e. g., V. F. Mukhanov, H. A. Feldman, and R. H. Brandenberger, Phys. Rep. **215**, 203 (1992).
- [10] A. Vilenkin, Phys. Rev. **D52**, 3365 (1995).
- [11] S. Winitzki and A. Vilenkin, Phys. Rev. **D53**, 4298 (1996).
- [12] A. D. Linde and A. Mezhlumian, Phys. Rev. **D53**, 4267 (1996).
- [13] A. Vilenkin, Phys. Rev. Lett. **81**, 5501 (1998).
- [14] M. Aryal and A. Vilenkin, Phys. Lett. **B199**, 351 (1987).
- [15] A.D. Linde, Phys. Lett. **B 327**, 208 (1994); A. Vilenkin, Phys. Rev. Lett. **72**, 3137 (1994).
- [16] J. Garriga and A. Vilenkin, Phys. Rev. **D57**, 2230 (1998).
- [17] A. A. Starobinsky, in *Lecture Notes in Physics Vol. 246* (Springer, Heidelberg, 1986).
- [18] A.S. Goncharov, A.D. Linde and V.F. Mukhanov, Int. J. Mod. Phys. **A2**, 561 (1987).
- [19] Y. Nambu and M. Sasaki, Phys. Lett. **B219**, 240 (1989); K. Nakao, Y. Nambu and M. Sasaki, Prog. theor. phys. **80**, 1041 (1988).
- [20] M. Mijic, Phys. Rev. **D42**, 2469 (1990).
- [21] D. S. Salopek and J. R. Bond, Phys. Rev. **D43**, 1005 (1991).
- [22] J. Garcia-Bellido, A. D. Linde, and D. A. Linde, Phys. Rev. **D50**, 730 (1994).
- [23] A. Vilenkin, Phys. Rev. **D59**, 123506 (1999).
- [24] A. A. Starobinsky and J. Yokoyama, Phys. Rev. **D50**, 6357 (1994).
- [25] A. D. Linde and D. A. Linde, Phys. Rev. **D50**, 2456 (1994).
- [26] A. Vilenkin and S. Winitzki, in preparation.
- [27] W. H. Press, S. A. Teukolsky, W.T. Vetterling and B. P. Flannery, *Numerical Recipes in C*, Cambridge University Press, 1993, chapter 2.
- [28] C. W. Gardiner, *Handbook of stochastic methods for physics, chemistry, and the natural sciences*, Springer-Verlag, Berlin, 1985.

FIGURES

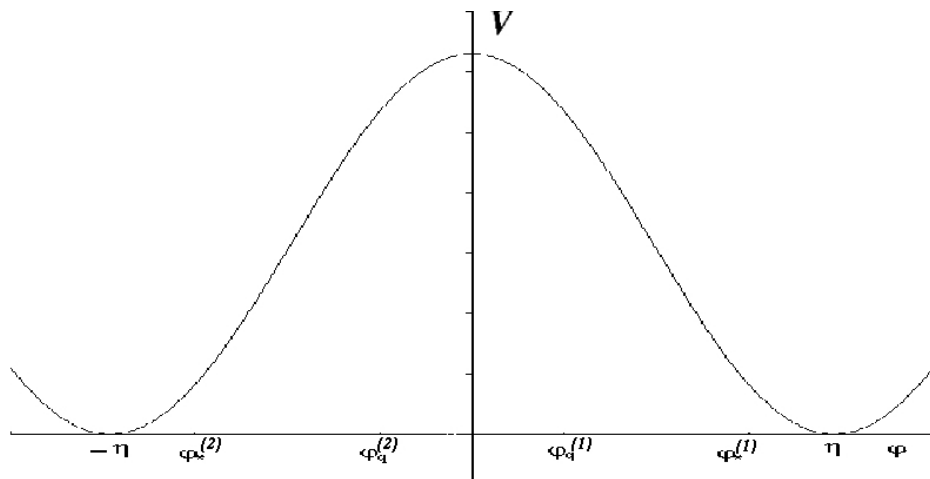


FIG. 1. The inflaton potential for the double-well model (8).

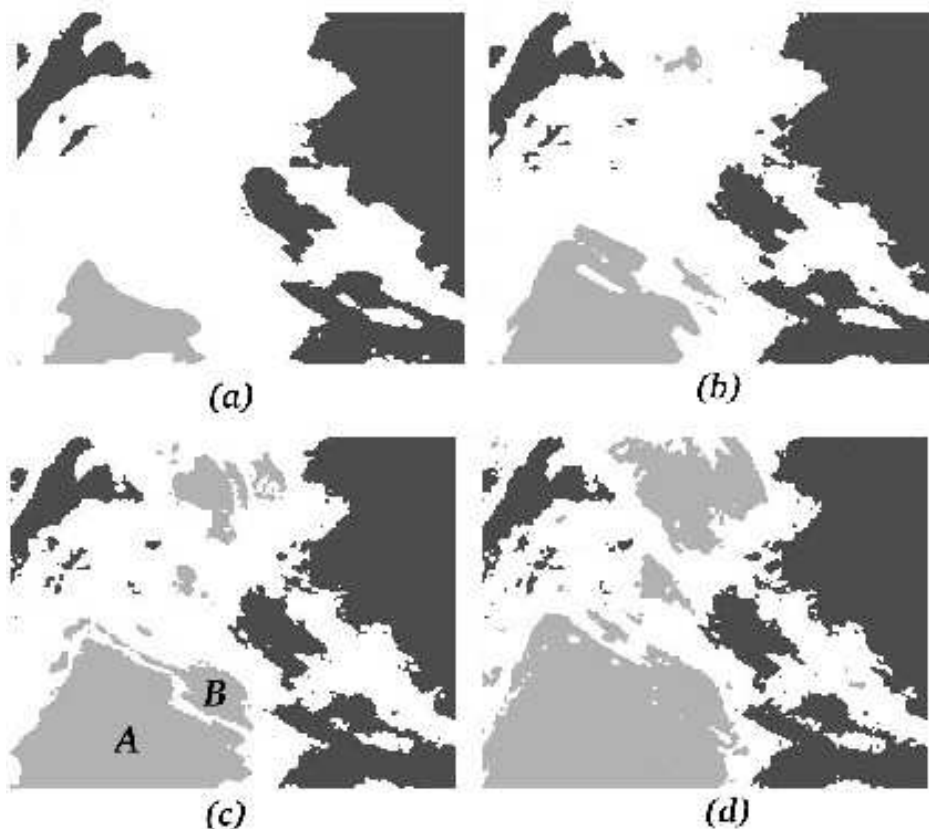


FIG. 2. A two-dimensional simulation for the double-well model at four consecutive moments of proper time: $t = 5H_0^{-1}$ (a), $t = 5.5H_0^{-1}$ (b), $t = 6H_0^{-1}$ (c), $t = 6.5H_0^{-1}$ (d). We evolved a comoving region of initial size $l = H_0^{-1}$ with the initial value of $\varphi = 0$ at $t = 0$. Inflating regions are shown white, while thermalized regions with $\varphi = +\eta$ and $\varphi = -\eta$ are shown with different shades of grey. Thermalized regions of the same type tend to join in the course of the simulation. For example, regions labeled A and B in snapshot (c) have merged into a single region in snapshot (d).

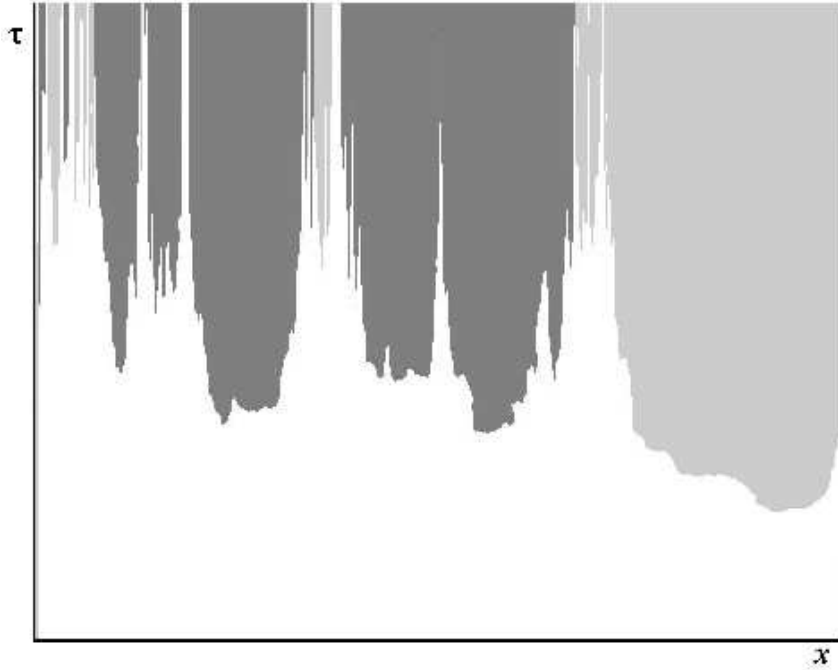


FIG. 3. Spacetime structure in a one-dimensional simulation for the double-well model. It can be thought of as a spacetime slice through the $(2 + 1)$ -dimensional simulation illustrated in Fig. 2. Inflating regions are white, and thermalized regions of different type are shown with different shades of grey.

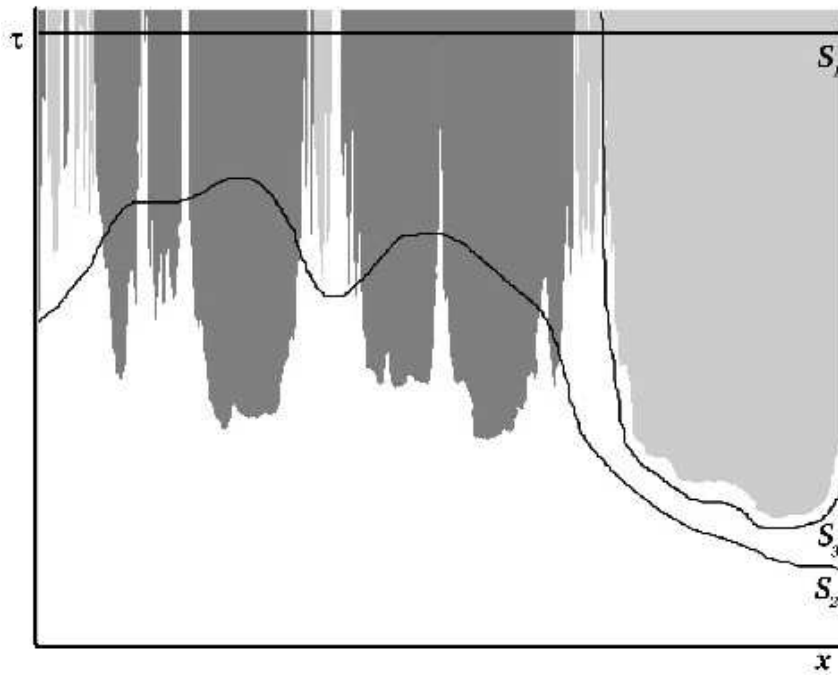


FIG. 4. \mathcal{S}_1 is a surface of a constant proper time. It crosses many thermalized regions of different types. \mathcal{S}_2 is a spacelike surface which crosses regions of only one type. \mathcal{S}_3 is a spacelike surface which does not cross any thermalized regions.

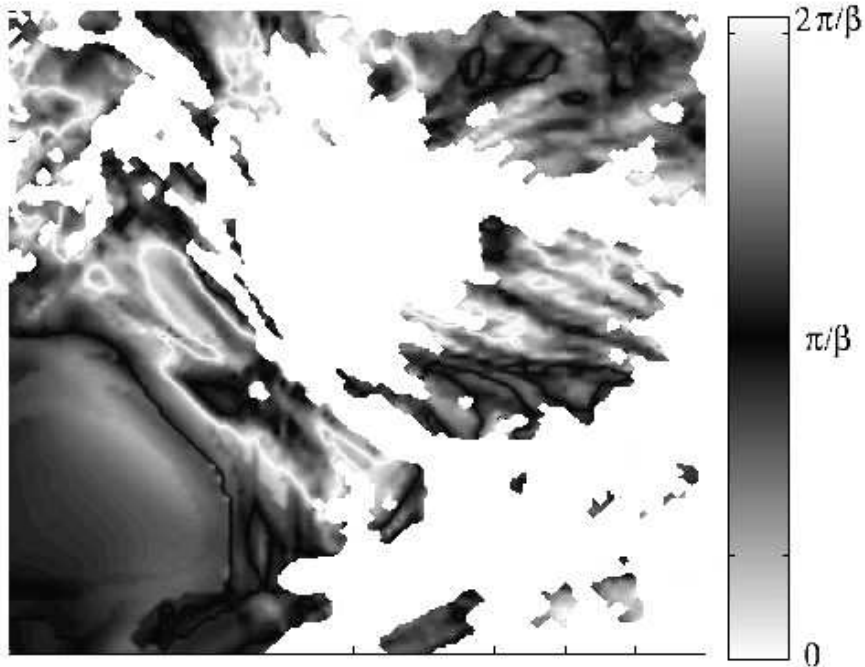


FIG. 5. A snapshot of a simulation for the two-field model (12). Inflating regions are white, while regions that thermalized with different values of χ are shown with different shades of grey. The shading code is indicated in the bar on the right of the figure.

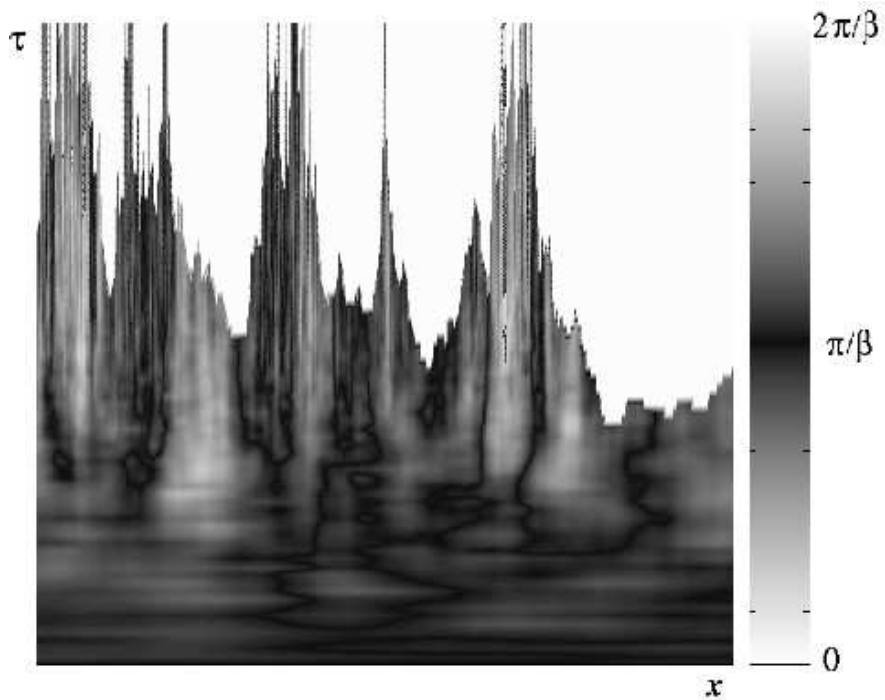


FIG. 6. Spacetime structure in a one-dimensional simulation for the two-field model showing the evolution of a comoving region of initial size $l = H_0^{-1}$ with initially homogeneous $\varphi = 0$ and $\chi = \pi/\beta$. The values of the field χ are indicated throughout the inflating region using the same shading code as in Fig. 5. The thermalized regions are left white.

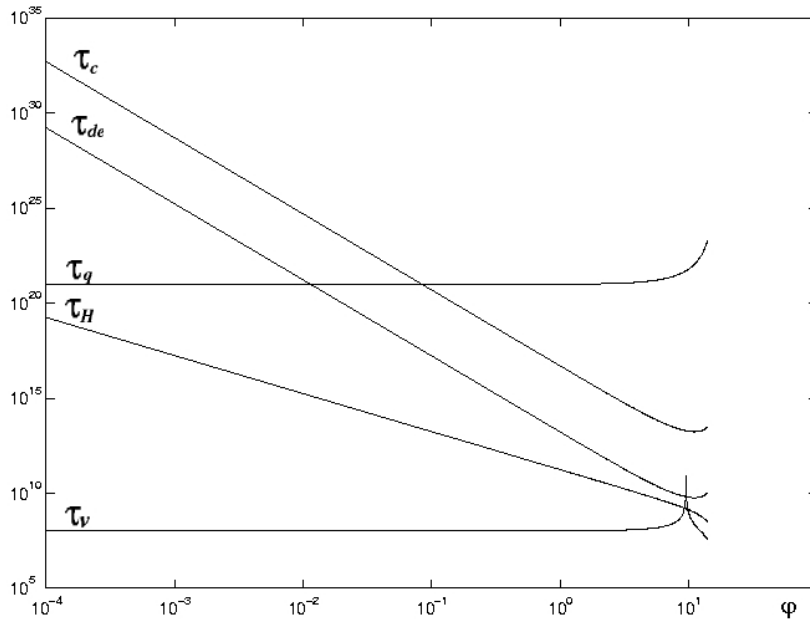


FIG. 7. The characteristic times as functions of φ for the model parameters (39).

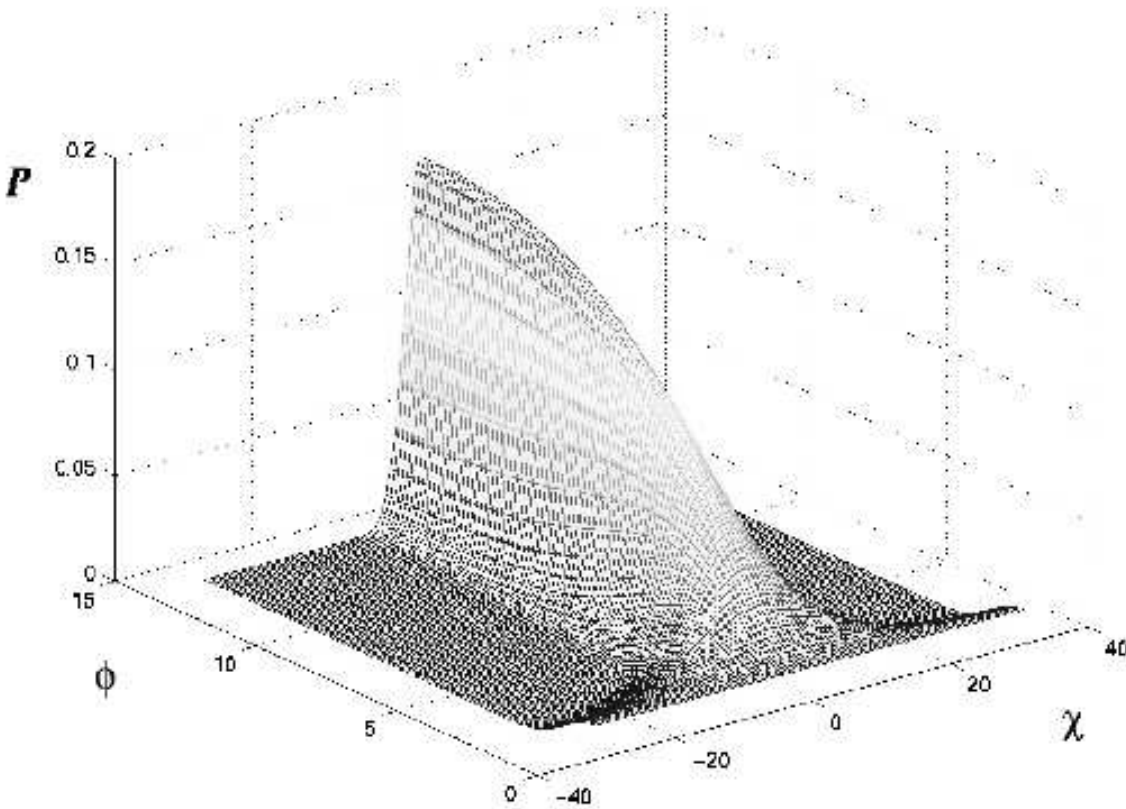


FIG. 8. The solution of the FP equation for the model parameters (39).

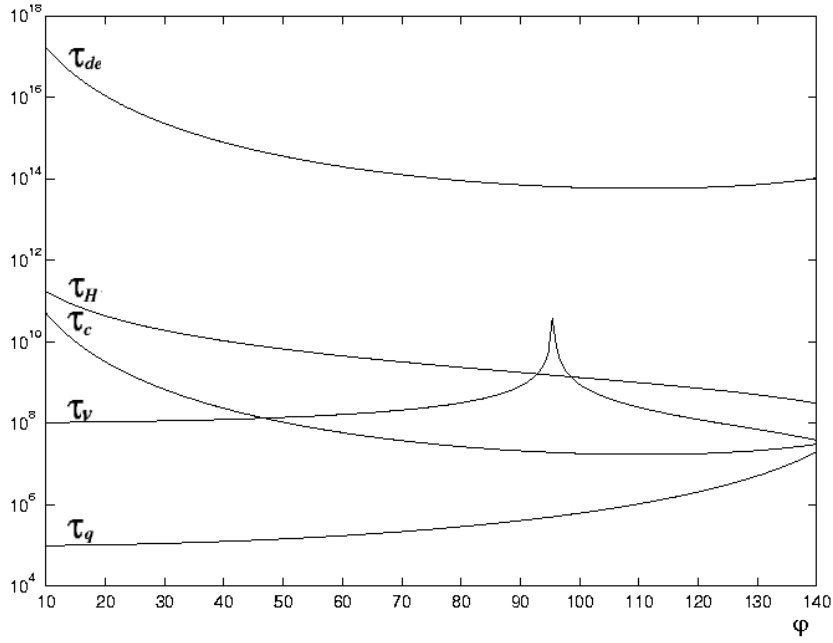


FIG. 9. The characteristic times as functions of φ for the model parameters (44).

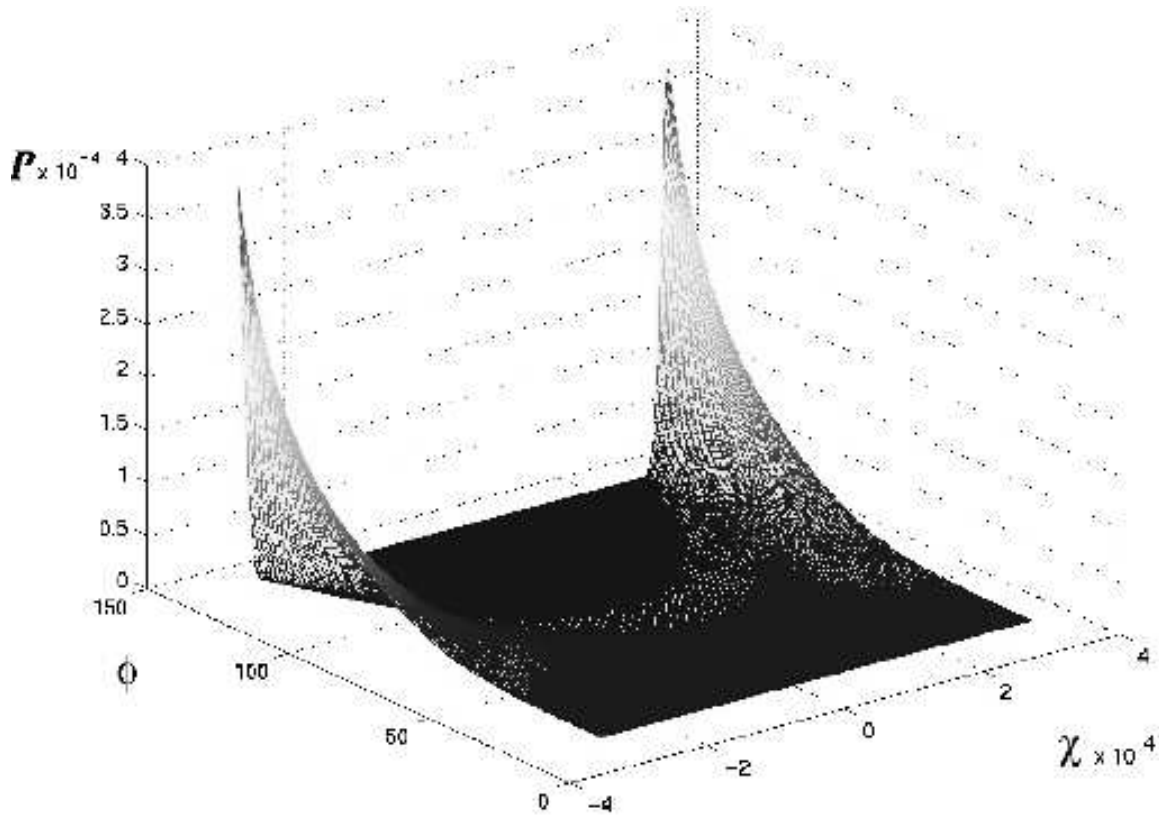


FIG. 10. The solution of the FP equation for the model parameters (44).

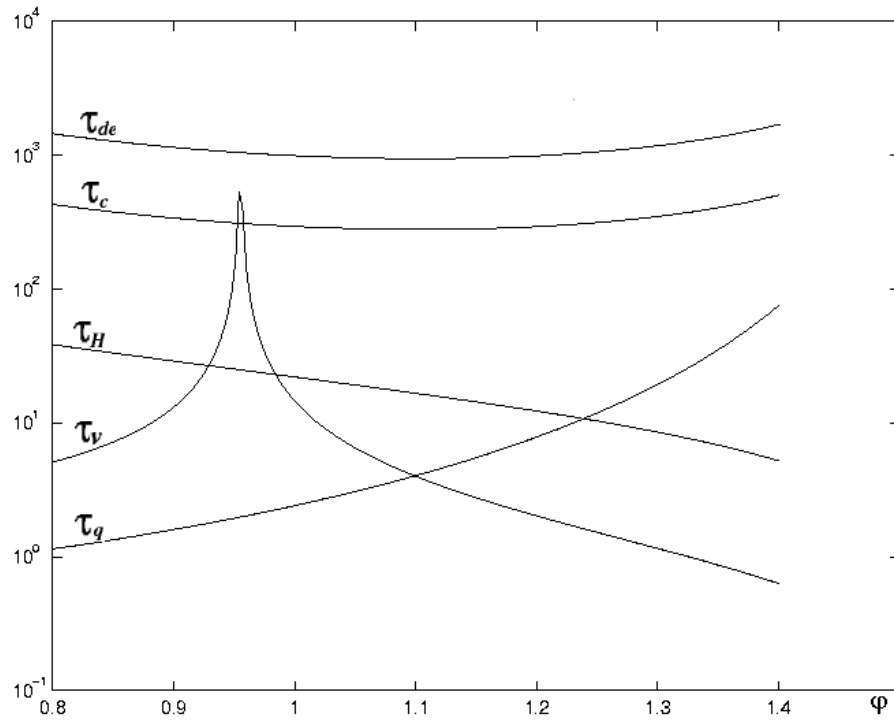


FIG. 11. The characteristic times as functions of φ for the model parameters (45).

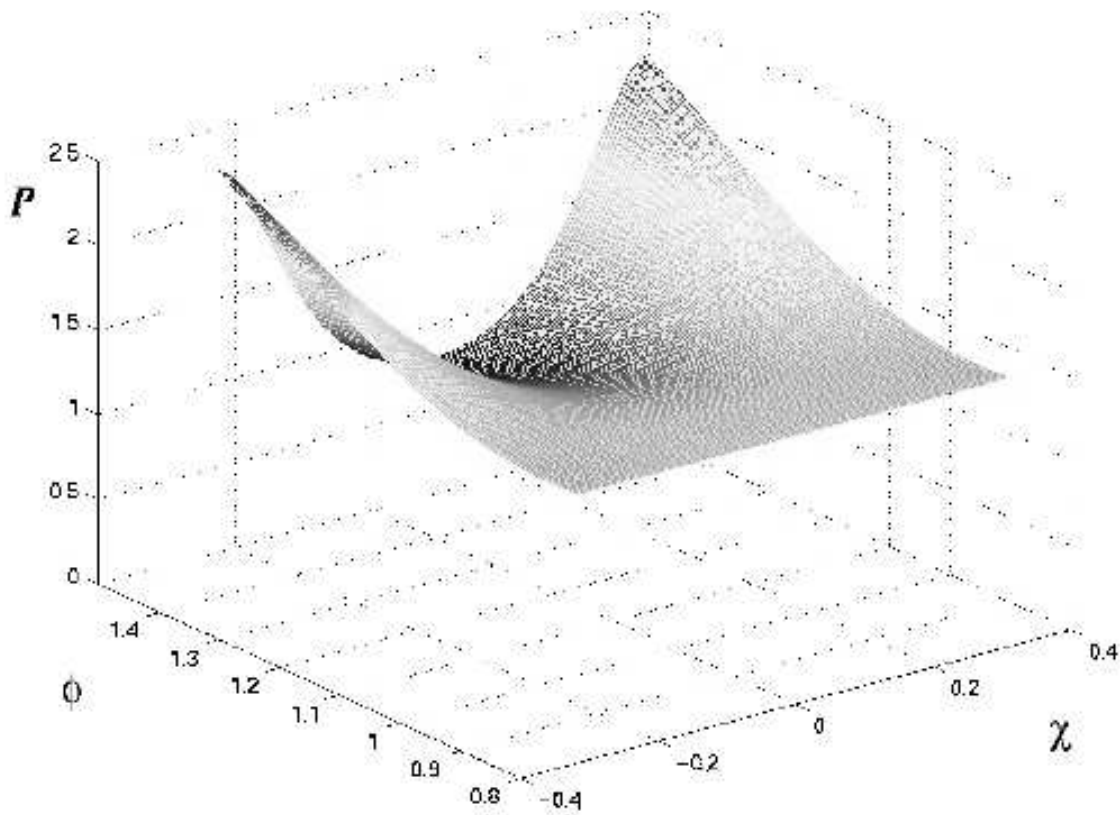


FIG. 12. The solution of the FP equation for the model parameters (45).

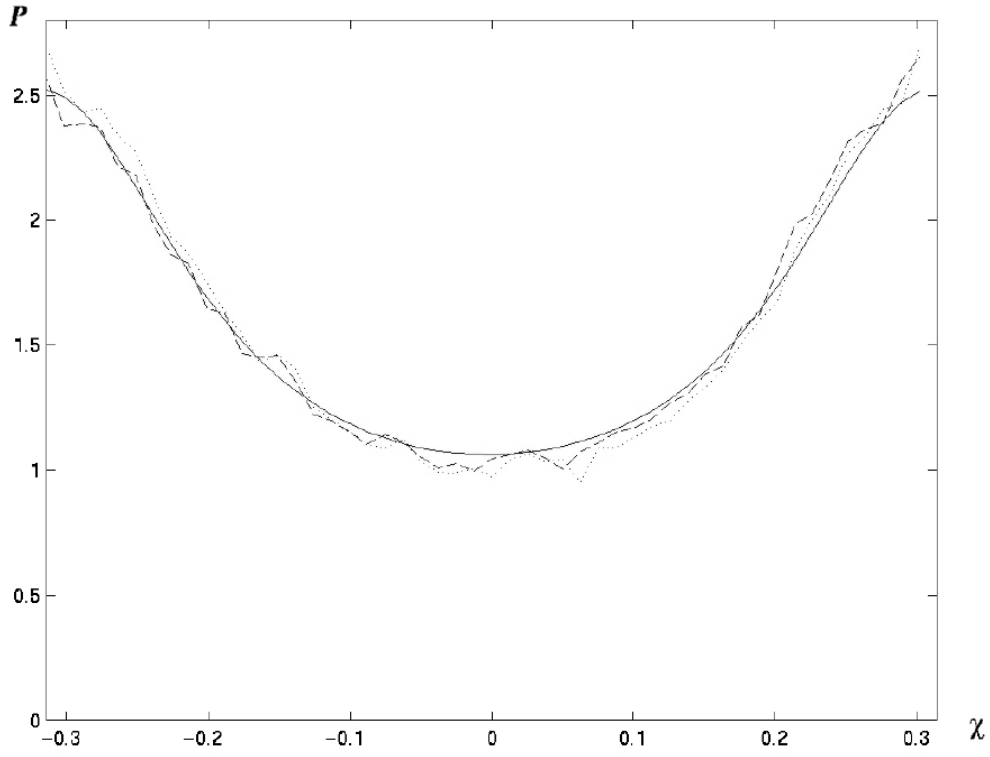


FIG. 13. The probability distribution for χ for the model parameters (45). The distributions obtained directly from two different thermalization lines in a simulation are shown by dotted and dashed lines. The solid line shows the distribution obtained by solving the FP equation.